EUROPEAN JOURNAL OF PURE AND APPLIED MATHEMATICS
2026, Vol. 19, Issue 2, Article Number 7575
ISSN 1307-5543 – ejpam.com
Published by New York Business Global

Identifying the Inverse Initial Condition for the Beam Equation Using Final-Time Condition

Shirin I. Mahmood[1,*], Shilan O. Hussein[1], Taysir E. Dyhoum[2,3]

[1] *Department of Mathematics, College of Science, University of Sulaimani, Sulaymaniyah, Kurdistan Region, Iraq*
[2] *Department of Computing and Mathematics, Faculty of Science and Engineering, Manchester Metropolitan University, Manchester, UK*
[3] *Department of Mathematics, Misurata University, Misurata, Libya*

Abstract. This paper explores an inverse problem related to the initial condition of the beam equation "a fourth-order partial differential equation" with mixed boundary conditions. The goal is to recover an unknown initial condition function using additional displacement data at the final time. We consider two types of inverse problems: one focusing on the inverse initial displacement and the other on the inverse initial velocity. This inverse initial problem is linear with a unique solution, but it is considered ill-posed because solutions may not exist for all input data. Even when solutions do exist, they might not depend continuously on the input. To achieve a stable numerical solution, we apply the finite difference method combined with Tikhonov regularization, testing various regularization orders. The regularization parameter is determined using the L-curve method and the norm error. Our numerical results demonstrate that this approach yields accurate solutions for exact data and stable results for noisy data. Although the literature describes conditions ensuring uniqueness and continuous dependence, it lacks numerical evidence. Thus, developing an efficient numerical method for this linear yet ill-posed problem is our main goal and contribution.

2020 Mathematics Subject Classifications: 35R30, 65N06, 65N21

Key Words and Phrases: Inverse initial displacement problem, inverse initial velocity problem, fourth-order partial differential equation, finite difference method, zero-order Tikhonov regularization.

---

1. Introduction

Inverse problems related to fourth-order partial differential equations play a vital role in many areas of mathematical physics. These problems are particularly important in

*Corresponding Author.
DOI: https://doi.org/10.29020/nybg.ejpam.v19i2.7575

Email addresses: `shirin.Mahmood@univsul.edu.iq` (S. I. Mahmood),
`shilan.husen@univsul.edu.iq` (S. O. Hussein), `t.dyhoum@mmu.ac.uk` (T. E. Dyhoum)

studying the bending and transverse vibrations of elastic beams and plates. From an engineering perspective, the beam equation serves as an effective model for understanding the mechanical behavior of structures such as bridges, aircraft components, and flexible systems [1–3]. This research mainly examines inverse problems where the initial conditions are unknown. Theoretical results on the existence and uniqueness of solutions for both direct and inverse problems are provided in [4, 5]. Besides these theoretical insights, developing effective numerical methods for solving inverse problems is crucial for progressing in numerical analysis and tackling real-world applications. Therefore, this study focuses on finding numerical solutions to these inverse problems. Additionally, comprehensive stability results for direct and inverse problems are thoroughly shown.

Inverse initial condition problems have attracted significant research interest. For the heat equation, many methods have been developed to estimate unknown initial conditions, as shown in references [6–9]. Regarding beam and vibration equations, studies [4, 5, 10, 11] explored inverse problems related to identifying initial conditions, source terms, coefficients, and kernels. Additionally, several studies, including references [12–17], have investigated using final-time displacement as an extra boundary condition for hyperbolic equations, while [18, 19] applied this approach to parabolic and other differential equations. Moreover, [5] used it for beam equations, where only the theoretical aspect was addressed. Recent research investigates beam-type equations from multiple perspectives. In [20], a time-fractional Euler–Bernoulli beam equation and an inverse problem for determining a time-dependent coefficient were studied, with numerical experiments supporting the existence and uniqueness of solutions. Nave (2020) [21] introduces the Differential Homotopy Analysis Method (DHAM) for solving ordinary differential equations, demonstrating improved agreement with simulations. Building on this, the current work tackles an inverse problem for the classical Euler–Bernoulli beam equation, developing a stable, efficient numerical approach using finite difference discretization and Tikhonov regularization.

Furthermore, from the literature, it can be noted that the wave equation, a second-order PDE, is generally simpler to solve numerically than the fourth-order beam equation. It offers easier implementation, lower computational costs, and better stability. Consequently, it yields accurate results with consistent spatial and temporal discretizations, even on relatively fine grids. Conversely, the beam equation's fourth-order derivatives require more stringent stability conditions, leading to increased computational resources and memory usage, and limiting the grid size; our temporal discretization was restricted to about 25 points or fewer. Additionally, its higher-order nature makes the beam equation more susceptible to high-frequency oscillations, which can cause instability in inverse problems. Hence, successfully applying Tikhonov regularization is especially crucial here.

This article explores two inverse problems related to a fourth-order partial differential equation with unknown initial conditions. The unknowns include the initial displacement and initial velocity, which require additional information obtained from solving a mixed initial-boundary value problem, as explained in Section 2. Both inverse problems are defined and analyzed, with numerical results presented in Sections 3 and 4, where finite difference methods are used as numerical techniques [22–24] to approximate both inverse problems.

Nomenclature

$\omega(x,t)$	Transverse displacement (unknown solution)
x,t	Space and time variables
Λ	Space–time domain
$\mathcal{L}$	Length of the spatial interval
$\mathcal{T}$	Final time
α	Physical parameter
$\mathcal{H}(x,t)$	Source term
$u_0(x)$	Initial displacement
$u_1(x)$	Initial velocity
$\zeta(x)$	Final displacement measurement (overdetermination data)
Δx	Spatial step size, $\Delta x = \dfrac{\mathcal{L}}{M}$
Δt	Time step, $\Delta t = \dfrac{\mathcal{T}}{N}$
h	Spatial step size (notation used in figures/tables)
M	Number of spatial subintervals (grid parameter)
N	Number of time steps (temporal grid size), typically $N = M^2$
x_i	Spatial grid points, $x_i = i\Delta x$
t_j	Time grid points, $t_j = j\Delta t$
i,j	Spatial/time indices
ω_i^j	Approximation of $\omega(x_i,t_j)$
k	Wave number (Von Neumann analysis)
ϕ	Phase, $\phi = i\Delta x$
δ	Amplification factor (Von Neumann analysis)
r	Scheme parameter, $r = \alpha^2 \dfrac{\Delta t^2}{\Delta x^4}$
ϵ_i	Additive noise at grid point x_i
$\zeta^{\epsilon}(x_i)$	Noisy measurement, $\zeta^{\epsilon}(x_i) = \zeta(x_i) + \epsilon_i$
p	Noise level (percentage)
A,B	Coefficient matrices of the discrete inverse problems
$\underline{u_0}$	Vector of unknown initial displacement samples
$\underline{u_1}$	Vector of unknown initial velocity samples

$\underline{b}^{\epsilon}$	Noisy data vector associated with ζ^{ϵ} (IP1)
$\underline{c}^{\eta}$	Noisy/perturbed data vector (IP2)
$(\cdot)^T$	Transpose operator
λ	Tikhonov regularization parameter
I	Identity matrix
RRMSE	Relative Root Mean Square Error

2. Mathematical formulations

We study an inverse problem involving the determination of an unknown initial condition and the transverse vibration $\omega(x,t)$ of a uniform beam of length $\mathcal{L}$. These quantities satisfy a fourth-order partial differential equation within the domain $\Lambda = \{(x,t)\ ;\ 0 < x < \mathcal{L},\ 0 < t < \mathcal{T}\}$,

$$\omega_{tt}(x,t) + \alpha^2 \omega_{xxxx}(x,t) = \mathcal{H}(x,t), \qquad (x,t) \in \Lambda, \tag{1}$$

subject to the initial conditions,

$$\omega(x,0) = u_0(x), \qquad 0 \le x \le \mathcal{L}, \tag{2}$$

$$\omega_t(x,0) = u_1(x), \qquad 0 \le x \le \mathcal{L}, \tag{3}$$

mixed boundary conditions,

$$\omega(0,t) = \omega(\mathcal{L},t) = \omega_{xx}(0,t) = \omega_{xx}(\mathcal{L},t) = 0, \quad 0 \le t \le \mathcal{T}, \tag{4}$$

and an overdetermination condition, which is the final displacement measurement

$$\omega(x,\mathcal{T}) = \zeta(x), \qquad 0 \le x \le \mathcal{L}, \tag{5}$$

In the direct problem, it is required to determine the function $\omega(x,t) \in C^{4,2}_{x,t}(\Lambda) \cap C^{2,1}_{x,t}(\overline{\Lambda})$ satisfying (1)-(4) for the given constants α, $\mathcal{L}$, $\mathcal{T}$ and the sufficiently smooth functions $u_0(x), u_1(x)$ and $\mathcal{H}(x,t)$.

In the inverse problem, this study investigates two types of inverse initial condition problems:

Inverse Problem 1 (IP1): When we consider (1), (3)-(5) as inverse initial displacement problems, our primary objective is to determine (ω, u_0) such that $u_0(x) \in C[0,\mathcal{L}]$.

Inverse Problem 2 (IP2): When problems (1), (2), (4), and (5) are assigned as inverse initial velocity problems, the aim is to accurately determine (ω, u_1), where $u_1(x) \in C[0,\mathcal{L}]$.

The theorems concerning the existence and uniqueness of the research problem are as follows. To ensure stability, we will carefully address this in the numerical procedure section, which was not discussed in previous literature. By highlighting this aspect, we will provide clear examples showing how to meet the conditions of the theorems and effectively clarify the concept of stability.

Theorem 1. *Existence and uniqueness for direct problem* (1)-(4)*: let* $\mathcal{L}, \mathcal{T} > 0$ *and set* $\Lambda = \{(x,t)\ ;\ 0 < x < \mathcal{L},\ 0 < t < \mathcal{T}\}$*. Consider the initial–boundary value problem* (1) *with initial conditions* (2) *and* (3) *and boundary conditions* (4)*. Assume that:*

- $u_0 \in C^5[0,\mathcal{L}], \quad u_0(0) = u_0(\mathcal{L}) = 0, \quad u_0''(0) = u_0''(\mathcal{L}) = 0, \quad u_0''''(0) = u_0''''(\mathcal{L}) = 0;$
- $u_1 \in C^3[0,\mathcal{L}], \quad u_1(0) = u_1(\mathcal{L}) = 0, \quad u_1''(0) = u_1''(\mathcal{L}) = 0;$
- $\mathcal{H} \in C(\overline{\Lambda}) \cap C_x^3(\overline{\Lambda}), \quad \mathcal{H}(0,t) = \mathcal{H}(\mathcal{L},t) = 0,\ \mathcal{H}_{xx}(0,t) = \mathcal{H}_{xx}(\mathcal{L},t) = 0,\ 0 \le t \le \mathcal{T}.$

Then there exists a unique classical solution $\omega : \Lambda \to \mathbb{R}$ *of the above problem. Moreover,*

$$\omega \in C^2\big([0,\mathcal{T}]; L^2(0,\mathcal{L})\big) \cap C^1\big([0,\mathcal{T}]; H^2(0,\mathcal{L})\big) \cap C^0\big([0,\mathcal{T}]; H^4(0,\mathcal{L})\big).$$

A comprehensive exposition of the proof of the above theorem is available in references [4, 5].

Theorem 2. *Existence and Uniqueness for* **IP1** (1) *and* (3)-(5)*: If the functions* $u_0(x)$ *and* $\zeta(x)$ *belong to the class* $C^{7+k}[0,\mathcal{L}]$*, where* $\varepsilon < k < 1$*, and satisfy* $u_0^{(i)}(0) = u_0^{(i)}(\mathcal{L}) = \zeta^{(i)}(0) = \zeta^{(i)}(\mathcal{L}) = 0$*,* $i = 0,2,4,6$*, then there exists a unique continuous solution of* **IP1***, and this solution is determined by the series "For a more detailed explanation of how the series is constructed, refer to equations (53) and (54) in [5]".*

Theorem 3. *Existence and Uniqueness for* **IP2** (1)*,* (2)*,* (4)*, and* (5)*: Assume that one of the following conditions is satisfied:*

(i) the function $\zeta(x)$ *belongs to the class* $C^5[0,\mathcal{L}]$ *and satisfies* $\zeta^{(i)}(0) = \zeta^{(i)}(\mathcal{L}) = 0,\ i = 0,2,4$*, and the function* $u_1(x)$ *belongs to the class* $\in C^3[0,\mathcal{L}]$ *and satisfies* $u_1^{(i)}(0) = u_1^{(i)}(\mathcal{L}) = 0,\ i = 0,2.$

(ii) the function $\zeta(x)$ *belongs to the class* $C^{7+k}[0,\mathcal{L}]$*,* $\varepsilon < k < 1$*, and satisfies* $\zeta^{(i)}(0) = \zeta^{(i)}(\mathcal{L}) = 0,\ i = 0,2,4,6$*, and the function* $u_1(x)$ *belongs to the class* $C^{5+k}[0,\mathcal{L}]$ *and satisfies* $u_1^{(i)}(0) = u_1^{(i)}(\mathcal{L}) = 0,\ i = 0,2,4.$

Then there exists a unique solution of **IP2***, which appears as the series, and to see how to construct and what the series looks like, see references [5] in equations (58) and (60).*

Sabitov (2020) [5] provided detailed proofs for both Theorem 2 and Theorem 3. In addition, section 4 presents the numerical results from Theorems 1–3, which outline the conditions for uniqueness and stability that guide the numerical scheme and data selection. Due to the problem being ill-posed, Tikhonov regularization with finite differences ensures stability. Experiments confirm the theory, demonstrating stability with noisy data and convergence with precise data. Overall, the results showcase a practical application of the framework.

3. Numerical procedure

This section explains how to select $N = M^2$ to guaranty stability, given that $\Delta t \leq \frac{\Delta x^2}{2\alpha}$, where $\Delta x = \frac{\mathcal{L}}{M}$ and $\Delta t = \frac{\mathcal{T}}{N}$. The intervals $(0, \mathcal{L})$ and $(0, \mathcal{T})$ are subdivided into points points M , respectively, with points defined as $x_i = i\Delta x$ for $0 \leq i \leq M$ and $t_j = j\Delta t$ for $0 \leq j \leq N$. We employ a fully explicit finite difference scheme based on second-order central differences [10, 14, 24]. Next, we discretize the direct problem (1)–(4) on a uniform grid. Specifically, the interval $[0, \mathcal{L}]$ is partitioned into equally spaced nodes x_i, and the numerical approximation is denoted by $\omega_i^j \approx \omega(x_i, t_j)$. The required derivatives are then approximated using standard second-order centered formulas; for example, the second-order time derivative is approximated by:

$$\omega_{tt}(x_i, t_j) \approx \frac{\omega_i^{j+1} - 2\omega_i^j + \omega_i^{j-1}}{\Delta t^2}, \qquad \omega_{xx}(x_i, t_j) \approx \frac{\omega_{i+1}^j - 2\omega_i^j + \omega_{i-1}^j}{(\Delta x)^2}.$$

Discretizing the term $(\omega_{xxxx}(x, t))$ is the most computationally intensive part of the beam equation. We will therefore outline the steps to illustrate how the formula is derived and implemented in MATLAB.
Step 1// Applying the second-derivative operator twice:

$$\omega_{xxxx}(x_i, t_j) = (\omega_{xx})_{xx}(x_i, t_j) \approx \frac{\omega_{xx}(x_{i+1}, t_j) - 2\omega_{xx}(x_i, t_j) + \omega_{xx}(x_{i-1}, t_j)}{(\Delta x)^2},$$

Step 2// Substituting the following equations into the above equation (Step 1)

$$\omega_{xx}(x_{i+1}, t_j) \approx \frac{\omega_{i+2}^j - 2\omega_{i+1}^j + \omega_i^j}{(\Delta x)^2}, \qquad \omega_{xx}(x_{i-1}, t_j) \approx \frac{\omega_i^j - 2\omega_{i-1}^j + \omega_{i-2}^j}{(\Delta x)^2},$$

we obtain

$$\omega_{xxxx}(x_i, t_j) \approx \frac{\omega_{i-2}^j - 4\omega_{i-1}^j + 6\omega_i^j - 4\omega_{i+1}^j + \omega_{i+2}^j}{(\Delta x)^4}, \qquad i = 2, \ldots, M-2.$$

This scheme achieves second-order spatial accuracy. The stencil used at an interior node is listed as follows:

$$\frac{1}{(\Delta x)^4}\begin{array}{c|ccccc} \text{Node} & i-2 & i-1 & i & i+1 & i+2 \\ \hline \text{Coefficient} & 1 & -4 & 6 & -4 & 1 \end{array}.$$

Step 3// Applying boundary condition:
at $x = 0$:

$$\omega(0, t_j) = 0, \Rightarrow \omega_0^j = 0; \quad \omega_{xx}(0, t_j) \approx \frac{\omega_1^j - 2\omega_0^j + \omega_{-1}^j}{(\Delta x)^2} = 0, \Rightarrow \omega_{-1}^j = -\omega_1^j,$$

at $x = \mathcal{L}$:

$$\omega(\mathcal{L}, t_j) = 0 \Rightarrow \omega_M^j = 0; \quad \omega_{xx}(\mathcal{L}, t_j) \approx \frac{\omega_{M+1}^j - 2\omega_M^j + \omega_{M-1}^j}{(\Delta x)^2} = 0, \Rightarrow \omega_{M+1}^j = -\omega_{M-1}^j.$$

Step 4// Next, we demonstrate how the final equation from step 2 is discretized for $i = 1$ and $i = M - 1$

$$\omega_{xxxx}(x_1, t_j) \approx \frac{\omega_{-1}^j - 4\omega_0^j + 6\omega_1^j - 4\omega_2^j + \omega_3^j}{(\Delta x)^4},\ i = 1$$

$\Rightarrow$ substituting $\omega_{-1}^j = -\omega_1^j$ and $\omega_0^j = 0$ gives

$$\omega_{xxxx}(x_1, t_j) \approx \frac{5\omega_1^j - 4\omega_2^j + \omega_3^j}{(\Delta x)^4}.$$

Similarly, at $i = M - 1$,

$$\omega_{xxxx}(x_{M-1}, t_j) \approx \frac{\omega_{M-3}^j - 4\omega_{M-2}^j + 6\omega_{M-1}^j - 4\omega_M^j + \omega_{M+1}^j}{(\Delta x)^4},$$

substituting $\omega_M^j = 0$ and $\omega_{M+1}^j = -\omega_{M-1}^j$ gives

$$\omega_{xxxx}(x_{M-1}, t_j) \approx \frac{\omega_{M-3}^j - 4\omega_{M-2}^j + 5\omega_{M-1}^j}{(\Delta x)^4}.$$

Step 5// In the direct problem, we discretized equations (1)-(4) and followed Steps 1–4 to create the final numerical scheme:

$$\begin{aligned}
&\omega_i^{j+1} = -r\omega_{i-2}^j + 4r\omega_{i-1}^j + (2-6r)\omega_i^j + 4r\omega_{i+1}^j - r\omega_{i+2}^j - \omega_i^{j-1} + \Delta t^2 \mathcal{H}_i^j \\
&\omega_1^{j+1} = 4r\omega_0^j + (2-5r)\omega_1^j + 4r\omega_2^j - r\omega_3^j - \omega_1^{j-1} + \Delta t^2 \mathcal{H}_1^j \\
&\omega_{M-1}^{j+1} = -r\omega_{M-3}^j + 4r\omega_{M-2}^j + (2-5r)\omega_{M-1}^j + 4r\omega_M^j - \omega_{M-1}^{j-1} + \Delta t^2 \mathcal{H}_{M-1}^j, \quad j = \overline{1, N-1}
\end{aligned}$$

$$\begin{aligned}
\omega_i^1 &= \frac{1}{2}\Big(- r\, u_0(x_{i-2}) + 4r\, u_0(x_{i-1}) + (2-6r)\, u_0(x_i) + 4r\, u_0(x_{i+1}) - r\, u_0(x_{i+2}) + \Delta t^2 \mathcal{H}_i^0 \Big) \\
&\quad + \Delta t\, u_1(x_i), \\
\omega_1^1 &= \frac{1}{2}\Big(4r\, u_0(x_0) + (2-5r)\, u_0(x_1) + 4r\, u_0(x_2) - r\, u_0(x_3) + \Delta t^2 \mathcal{H}_1^0 \Big) + \Delta t\, u_1(x_1), \\
\omega_{M-1}^1 - \Delta t\, u_1(x_{M-1}) &= \frac{1}{2}\Big(- r\, u_0(x_{M-3}) + 4r\, u_0(x_{M-2}) + (2-5r)\, u_0(x_{M-1}) + 4r\, u_0(x_M) \\
&\qquad + \Delta t^2 \mathcal{H}_{M-1}^0 \Big) + \Delta t\, u_1(x_{M-1}), \quad j = 0.
\end{aligned}$$

where $r = \alpha^2 \dfrac{\Delta t^2}{\Delta x^4}$, $\mathcal{H}_i^j \approx \mathcal{H}(x_i, t_j)$, $\omega_i^0 = u_0(x_i)$, $i = \overline{0, M}$, $\frac{\omega_i^1 - \omega_i^{-1}}{2\Delta t} = u_1(x_i)$, $i = \overline{1, (M-1)}$, $j = \overline{0, N}$.

In order to derive additional conditions (5) numerically as follows, the equations above are implemented in MATLAB using loops or linear system matrices code

$$u(x_i, \mathcal{T}) = \zeta(x_i) \ \rightarrow \ u_i^{\mathcal{T}} = \zeta_i, \quad i = \overline{1, M}. \tag{6}$$

Step 6// Furthermore, both inverse problems (**IP1** and **IP2**) will be discretized using the following approach:
In the inverse initial displacement problem **IP1** ((1), (3)-(5)), the goal is to identify the function $\omega(x_i, t_j) = \omega_i^j$ and the initial displacement $u_0(x, 0) = u_0(x_i) = u_{0i}$, $i = \overline{2, M-2}$ and

$$\begin{aligned}
&\omega_i^{j+1} = -r\omega_{i-2}^j + 4r\omega_{i-1}^j + (2-6r)\omega_i^j + 4r\omega_{i+1}^j - r\omega_{i+2}^j - \omega_i^{j-1} + \Delta t^2 \mathcal{H}_i^j \\
&\omega_1^{j+1} = 4r\omega_0^j + (2-5r)\omega_1^j + 4r\omega_2^j - r\omega_3^j - \omega_1^{j-1} + \Delta t^2 \mathcal{H}_1^j \\
&\omega_{M-1}^{j+1} = -r\omega_{M-3}^j + 4r\omega_{M-2}^j + (2-5r)\omega_{M-1}^j + 4r\omega_M^j - \omega_{M-1}^{j-1} + \Delta t^2 \mathcal{H}_{M-1}^j, \quad j = \overline{2, N-1}
\end{aligned}$$

$$\begin{aligned}
&\omega_i^2 + u_0(x_i) = -r\omega_{i-2}^1 + 4r\omega_{i-1}^1 + (2-6r)\omega_i^1 + 4r\omega_{i+1}^1 - r\omega_{i+2}^1 + \Delta t^2 \mathcal{H}_i^1 \\
&\omega_1^2 + u_0(x_1) = 4r\omega_0^1 + (2-5r)\omega_1^1 + 4r\omega_2^1 - r\omega_3^1 + \Delta t^2 \mathcal{H}_1^1 \\
&\omega_{M-1}^2 + u_0(x_{M-1}) = -r\omega_{M-3}^1 + 4r\omega_{M-2}^1 + (2-5r)\omega_{M-1}^1 + 4r\omega_M^1 + \Delta t^2 \mathcal{H}_{M-1}^1, \quad j = 1
\end{aligned}$$

$$\begin{aligned}
&\omega_i^1 - \frac{1}{2}(-r\,u_0(x_{i-2}) + 4r\,u_0(x_{i-1}) + (2-6r)\,u_0(x_i) + 4r\,u_0(x_{i+1}) - r\,u_0(x_{i+2})) = \Delta t\,u_1(x_i) + \frac{1}{2}\Delta t^2 \mathcal{H}_i^0 \\
&\omega_1^1 - \frac{1}{2}(4r\,u_0(x_0) + (2-5r)\,u_0(x_1) + 4r\,u_0(x_2) - r\,u_0(x_3)) = \Delta t\,u_1(x_1) + \frac{1}{2}\Delta t^2 \mathcal{H}_1^0 \\
&\omega_{M-1}^1 - \frac{1}{2}(-r\,u_0(x_{M-3}) + 4r\,u_0(x_{M-2}) + (2-5r)\,u_0(x_{M-1}) + 4r\,u_0(x_M)) = \Delta t\,u_1(x_{M-1}) + \\
&\frac{1}{2}\Delta t^2 \mathcal{H}_{M-1}^0, \quad j = 0.
\end{aligned}$$

In addressing the inverse initial velocity problem **IP2** ((1), (2), (4), and (5)), we can effectively determine the unknowns (ω_i^j, u_{1i}), $i = \overline{2, M-2}$ through the following steps:

$$\begin{aligned}
&\omega_i^{j+1} = -r\omega_{i-2}^j + 4r\omega_{i-1}^j + (2-6r)\omega_i^j + 4r\omega_{i+1}^j - r\omega_{i+2}^j - \omega_i^{j-1} + \Delta t^2 \mathcal{H}_i^j \\
&\omega_1^{j+1} = 4r\omega_0^j + (2-5r)\omega_1^j + 4r\omega_2^j - r\omega_3^j - \omega_1^{j-1} + \Delta t^2 \mathcal{H}_1^j, \\
&\omega_{M-1}^{j+1} = -r\omega_{M-3}^j + 4r\omega_{M-2}^j + (2-5r)\omega_{M-1}^j + 4r\omega_M^j - \omega_{M-1}^{j-1} + \Delta t^2 \mathcal{H}_{M-1}^j, \quad j = \overline{1, N-1}
\end{aligned}$$

$$\begin{aligned}
&\omega_i^1 - \Delta t\,u_1(x_i) = \frac{1}{2}\Big(-r\,u_0(x_{i-2}) + 4r\,u_0(x_{i-1}) + (2-6r)\,u_0(x_i) + 4r\,u_0(x_{i+1}) - r\,u_0(x_{i+2}) + \Delta t^2 \mathcal{H}_i^0 \Big), \\
&\omega_1^1 - \Delta t\,u_1(x_1) = \frac{1}{2}\Big(4r\,u_0(x_0) + (2-5r)\,u_0(x_1) + 4r\,u_0(x_2) - r\,u_0(x_3) + \Delta t^2 \mathcal{H}_1^0 \Big), \\
&\omega_{M-1}^1 - \Delta t\,u_1(x_{M-1}) = \frac{1}{2}\Big(-r\,u_0(x_{M-3}) + 4r\,u_0(x_{M-2}) + (2-5r)\,u_0(x_{M-1}) + 4r\,u_0(x_M) + \Delta t^2 \mathcal{H}_{M-1}^0 \Big), \\
&\qquad j = 0.
\end{aligned}$$

After discretizing both inverse problems with over-determination condition (6), we create a linear system with $(M-1) \times N + M$ equations and $(M-1) \times N + (M-1)$ unknowns, where $N = M^2$. Given the large size of the system, the program cannot process the entire data set at once. Fortunately, because the system is linear, we can eliminate the unknowns ω_i^j in **IP1** and **IP2**, effectively simplifying the calculations. This reduces the computational complexity significantly. As a result, the simplified system consists of M equations and $M^2 - 1$ unknowns, as shown below:

$$\textbf{IP1}: \quad A\underline{u_0} = \underline{b}, \tag{7}$$

$$\textbf{IP2}: \quad B\underline{u_1} = \underline{c}, \tag{8}$$

Step 7// To analyze stability, we introduce a small perturbation $(\epsilon_i)_{\overline{i=1,M}}$ to the additional condition (6), the main contribution of this research, which has not been explored before. We use the Gaussian normal distribution, implemented in MATLAB with the "normrd" function, where mean zero, standard deviation $\sigma = p \times max_{x\in[0,\mathcal{L}]}|\zeta(x)|$ and p is the noise percentage:

$$\zeta^{\epsilon}(x_i) = \zeta(x_i) + \epsilon_i \;\rightarrow\; \zeta_i^{\epsilon} = \zeta_i + \epsilon_i \quad i = \overline{1, M}. \tag{9}$$

The vectors on the right side of equations (7) and (8) significantly impact the noisy measurements in (9), as illustrated below:

$$\textbf{IP1}: \quad A\underline{u_0} = \underline{b}^{\epsilon}, \tag{10}$$

$$\textbf{IP2}: \quad B\underline{u_1} = \underline{c}^{\eta}. \tag{11}$$

Consequently, the least-squares method can be employed to obtain an approximate solution to these overdetermined systems. For the systems of equations (10) and (11), the least-squares solution is given by:

$$\textbf{IP1}: \quad \underline{u_0} = (A^T A)^{-1} A^T \underline{b}^{\epsilon}, \tag{12}$$

$$\textbf{IP2}: \quad \underline{u_1} = (B^T B)^{-1} B^T \underline{c}^{\eta}, \tag{13}$$

where the superscript ^{T} and $^{-1}$ indicates the matrix transpose and inverse.

3.1. Stability analysis

The Von Neumann stability analysis is employed to validate this, assuming $\mathcal{H}(x,t) = 0$, $\omega_{xxxx}(x_i, t_j) = \frac{\omega_{i-2}^j - 4\omega_{i-1}^j + 6\omega_i^j - 4\omega_{i+1}^j + \omega_{i+2}^j}{\Delta x^4}$, $\omega_{tt}(x_i, t_j) = \frac{\omega_i^{j+1} - 2\omega_i^j + \omega_i^{j-1}}{\Delta t^2}$, and let $\omega_i^j = \delta^j e^{ik\phi}$ such that $\phi = i\Delta x$, δ =amplification factor, and k =wave number. After applying the central finite difference method to formula (1), we get:

$$\omega_i^{j+1} - 2\omega_i^j + \omega_i^{j-1} = \frac{-\alpha^2 \Delta t^2}{\Delta x^4}(\omega_{i+2}^j - 4\omega_{i+1}^j + 6\omega_i^j - 4\omega_{i-1}^j + \omega_{i-2}^j),$$

then using $\omega_i^j = \delta^j e^{ik\phi}$ the above equation will be as follows:

$$\delta^{j+1} e^{ik\phi} - 2\delta^j e^{ik\phi} + \delta^{j-1} e^{ik\phi} = \frac{-\alpha^2 \Delta t^2}{\Delta x^4}(\delta^j e^{(i+2)k\phi} - 4\delta^j e^{(i+1)k\phi} + 6\delta^j e^{ik\phi} - 4\delta^j e^{(i-1)k\phi} + \delta^j e^{(i-2)k\phi}),$$

Next, divide both sides of the equation by $e^{ik\phi}$ and apply Euler's Formula to convert the exponential into cosine.

$$\delta^{j+1} - 2\delta^{j} + \delta^{j-1} = \frac{-\alpha^2 \Delta t^2}{\Delta x^4}(2\cos(2\theta) - 8\cos\theta + 6)\delta^{j}, \text{ where } \theta = k\phi, \text{ and divide both sides by } \delta^{j}$$

$$\delta - 2 + \delta^{-1} = \frac{-\alpha^2 \Delta t^2}{\Delta x^4}(2\cos(2\theta) - 8\cos\theta + 6) = -\alpha^2\Delta t^2\lambda, \Rightarrow \delta + \delta^{-1} = 2 - \alpha^2\Delta t^2\lambda,$$

where $\lambda = \frac{2\cos(2\theta) - 8\cos\theta + 6}{\Delta x^4}$, and for stability is require $|\delta| \leq 1 \Leftrightarrow |2 - \alpha^2\Delta t^2\lambda| \in [-2, 2] \Rightarrow |2 - \alpha^2\Delta t^2\lambda| \leq 2 \Rightarrow 0 \leq 2 - \alpha^2\Delta t^2\lambda \leq 4 \Rightarrow \Delta t \leq \frac{2}{\alpha\sqrt{\lambda}} \rightarrow \Delta t \leq \frac{\Delta x^2}{2\alpha}$.

If Δt is very small, causing $2 - \alpha^2\Delta t^2\lambda$ to be close to 2, then δ approaches 1, requiring $N = M^2$, which slows down oscillations. This demonstrates that stability depends on λ.

4. Numerical example

This section presents a numerical example, where $\Lambda = \{0 < x < 2\pi,\, 0 < t < 1\}$, demonstrating the application of all conditions from theorems 1, 2, and 3, using the following input data:

$$\mathcal{H}(x,t) = (2e^{t} + 1)2\sin(x), \quad x \in [0, 2\pi],\ t \in [0, 1], \tag{14}$$

$$\zeta(x) = 2(e + 1)\sin(x), \quad x \in [0, 2\pi]. \tag{15}$$

The exact solution is given by:

$$\omega(x,t) = 2(e^{t} + 1)\sin(x), \quad x \in (0, 2\pi),\ t \in (0, 1), \tag{16}$$

$$u_0(x) = 4\sin(x), \quad x \in [0, 2\pi], \tag{17}$$

$$u_1(x) = 2\sin(x), \quad x \in [0, 2\pi]. \tag{18}$$

To verify the expected second-order convergence of the numerical solution for the direct beam problem, a mesh refinement study is conducted using initial (17) and (18) and boundary conditions, along with the exact solution for $\omega(x,t)$ (16). Numerical solutions are computed on progressively refined spatial grids with $M = 64, 128, 256$, and 512. The grid spacing is $\Delta x = \frac{2\pi}{M}$, and the time step is $\Delta t = 0.8 \times \frac{(\Delta x)^2}{2}$, with $\alpha = 1$. Errors are then measured at $\mathcal{T} = 1$ using the maximum norm $E_\infty(\Delta x) = \max_i |\omega_{num}(x_i, \mathcal{T}) - \omega_{exact}(x_i, \mathcal{T})|$. The convergence rate $q = \log_2\left(\frac{E(\Delta x)}{E(\Delta x/2)}\right)$ is subsequently calculated. Results are summarized in Table 1. The Table 1 shows that halving the mesh size (Δx) decreases the error by about a factor of four, confirming that the computed rate is $q = 2$. Additionally, the infinity-norm error (E_∞) consistently reduces as the mesh is refined. These results support the expected second-order convergence of the direct solver when using the chosen stability-preserving refinement strategy.

Before adding noise, we numerically compute u_0 in **IP1** using equation (7) and compare it with the exact solution given in equation (17) for $M \in \{5, 10, 20, 30\}$ and $N \in \{10, 100, 400, 900\}$. Similarly, in **IP2**, we calculate u_1 using equation (8) and compare it

Table 1: Mesh refinement results for the direct beam problem with $\alpha = 1$ using $\Delta t = 0.8\,\Delta x^2/2$ and $\Delta x = 2\pi/M$.

M	$\Delta x = \dfrac{2\pi}{M}$	$\Delta t = 0.8\,\dfrac{\Delta x^2}{2}$	E_∞	q
64	9.81748×10^{-2}	3.84615×10^{-3}	3.6159×10^{-3}	–
128	4.90874×10^{-2}	9.63390×10^{-4}	9.0546×10^{-4}	1.9976
256	2.45437×10^{-2}	2.40910×10^{-4}	2.2646×10^{-4}	1.9994
512	1.22718×10^{-2}	6.02370×10^{-5}	5.6621×10^{-5}	1.9999

with the exact solution in equation (18), with $M \in \{5, 10, 15, 20\}$ and $N \in \{10, 100, 225, 400\}$. As shown in Figure 1, we observe good approximations in both problems: Figure 1(a) shows u_0, while Figure 1(b) displays u_1. To evaluate stability, noise levels $p \in \{1, 3, 5\}\%$

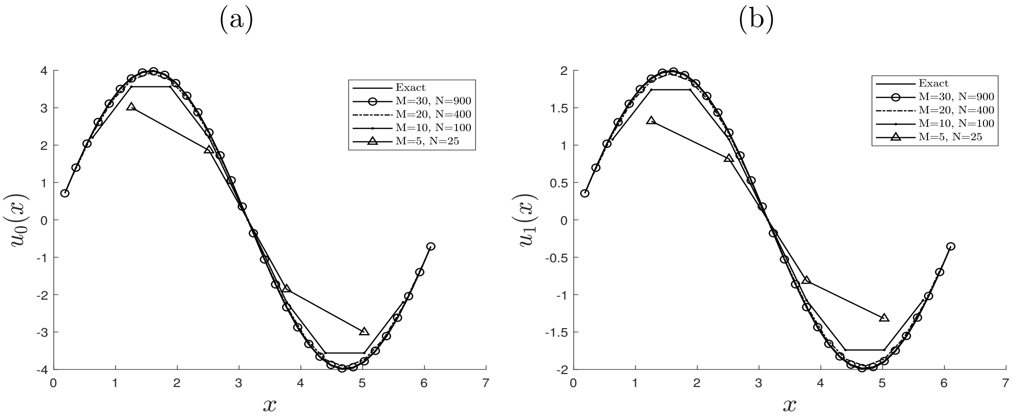

Figure 1: The exact solution for the initial condition (a) **IP1:** $u_0(x)$ equation (17), where $M \in \{5, 10, 20, 30\}$ and $N \in \{10, 100, 400, 900\}$, and (b) **IP2:** $u_1(x)$ equation (18), at $M \in \{5, 10, 15, 20\}$ and $N \in \{10, 100, 225, 400\}$, in comparison with the numerical solution (7) and (8), respectively.

are introduced as in equation (9). We calculate u_0 using equation (12) in **IP1** and u_1 using equation (13) in **IP2**, with $M = 25$ and $N = 625$, then compare these results with the exact solution. Figure 2 shows this comparison, clearly indicating that even small noise greatly affects the solution and causes instability. This demonstrates that the inverse problem is ill-posed: despite meeting the conditions for existence and uniqueness outlined in the theorems, the solution lacks stability. We also examine the relative root mean square error (RRMSE) of the functions $u_0(x)$ and $u_1(x)$ at different noise levels p to assess how increased noise affects the accuracy and stability of the reconstructed functions. The RRMSE for $u_0(x)$ (**IP1**) and $u_1(x)$ (**IP2**) is defined, respectively, by

$$\textbf{IP1: } \mathrm{RRMSE}(u_0(x)) = \frac{\| u_0(x)_{\text{num}} - u_0(x)_{\text{exact}} \|_2}{\| u_0(x)_{\text{exact}} \|_2} = \frac{\sqrt{\sum_{i=1}^{M-1} \left(u_0(x_i)_{\text{num}} - u_0(x_i)_{\text{exact}} \right)^2}}{\sqrt{\sum_{i=1}^{M-1} \left(u_0(x_i)_{\text{exact}} \right)^2}}, \tag{19}$$

$$\textbf{IP2: } \mathrm{RRMSE}(u_1(x)) = \frac{\|u_1(x)_{\text{num}} - u_1(x)_{\text{exact}}\|_2}{\|u_1(x)_{\text{exact}}\|_2} = \frac{\sqrt{\sum_{i=1}^{M-1}\left(u_1(x_i)_{\text{num}} - u_1(x_i)_{\text{exact}}\right)^2}}{\sqrt{\sum_{i=1}^{M-1}\left(u_1(x_i)_{\text{exact}}\right)^2}}, \tag{20}$$

where $\|\cdot\|_2$ is the discrete ℓ^2-norm. As shown in Table 2, the reconstruction error significantly rises with increasing noise levels for both functions. When there is no noise ($p = 0\%$), the relative root mean square error (RRMSE) remains low: 0.010857 for $u_0(x)$ and 0.014030 for $u_1(x)$, indicating precise recovery. However, even a small amount of noise (1%) causes a sharp increase in error, with RRMSE rising quickly at 3% and 5% noise levels. Notably, the errors for $u_1(x)$ are much larger than those for $u_0(x)$, showing that reconstructing $u_1(x)$ is more sensitive to noise. These findings emphasize the strong instability of the inverse problem and confirm its ill-posed nature, especially when measurement noise is present. We employ zero-order Tikhonov regularization to stabilize the

Table 2: RRMSE for the (a) $u_0(x)$ (**IP1**) and (b) $u_1(x)$ (**IP2**) under different noise levels $p = 0\%, 1\%, 3\%, 5\%$.

(a) $u_0(x)$

Noise level	RRMSE
$p = 0\%$	0.010857
$p = 1\%$	0.197779
$p = 3\%$	0.592070
$p = 5\%$	0.986519

(b) $u_1(x)$

Noise level	RRMSE
$p = 0\%$	0.014030
$p = 1\%$	6.518683
$p = 3\%$	19.555984
$p = 5\%$	32.593293

(a) (b)

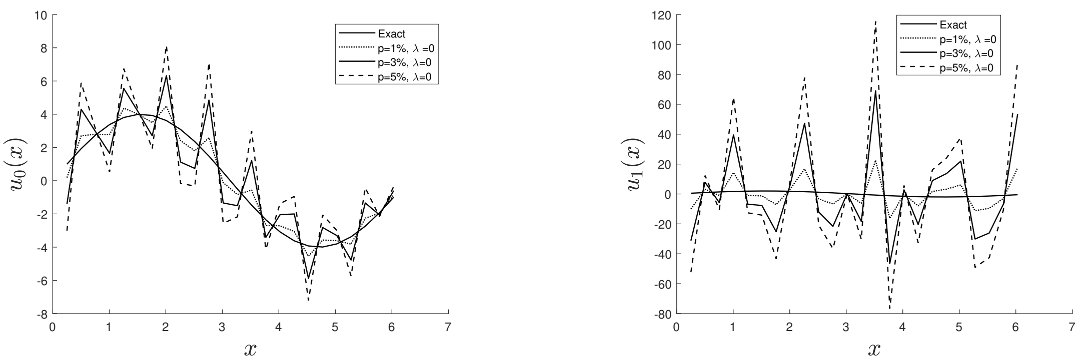

Figure 2: Comparison between noisy data for the initial condition (a) **IP1:** exact solution $u_0(x)$ (equation (17)) and numerical solution (equation (12)), and (b) **IP2:** exact solution $u_1(x)$ (equation (18)) and numerical solution (equation (13)), for $M = 25$, $N = 625$, and $p = \{1, 3, 5\}\%$.

results:

$$\textbf{IP1}: \quad \underline{u_0} = (A^T A + \lambda I)^{-1} A^T \underline{b}^{\epsilon}, \tag{21}$$

$$\textbf{IP2}: \quad \underline{u_1} = (B^T B + \lambda I)^{-1} B^T \underline{c}^{\eta}. \tag{22}$$

In this analysis, I represents the identity matrix, and λ refers to the regularization parameter. The least-squares formulations in Equations (12)-(13) utilize normal equations that may be unstable due to the ill-conditioning of matrix $A^T A$ and $B^T B$, especially in the beam equation. Small data disturbances can cause errors, which appear as oscillations in Figure 2. To address instability, we apply zero-order Tikhonov regularization (see Equations (21)-(22)). It enhances conditioning by replacing $A^T A$ and $B^T B$ with $A^T A + \lambda I$ and $B^T B + \lambda I$, stabilizing the inversion. It reduces noise amplification, is easy to implement, and results in a less computationally intensive linear system compared to a full singular value decomposition (SVD) method. Several values of λ are tested to achieve a stable and accurate solution. Among these, the optimal λ is determined by evaluating the norm error function of u_0 (23) in **IP1** and u_1 (24) in **IP2** with respect to λ. The value of λ that corresponds to the minimum error is chosen as the best regularization parameter. As illustrated in Figure 3 for **IP1** and Figure 4 for **IP2**, the minimum error is indicated by arrows. Figure 2 further confirms that this λ value, which leads to the minimum error, provides the optimal solution:

$$\textbf{IP1}: \quad \|u_0(x)_{\text{num}} - u_0(x)_{\text{exact}}\| = \left(\sum_{i=1}^{M} |u_0(x_i)_{\text{num}} - u_0(x_i)_{\text{exact}}|^2 \right)^{\frac{1}{2}}, \tag{23}$$

$$\textbf{IP2}: \quad \|u_1(x)_{\text{num}} - u_1(x)_{\text{exact}}\| = \left(\sum_{i=1}^{M} |u_1(x_i)_{\text{num}} - u_1(x_i)_{\text{exact}}|^2 \right)^{\frac{1}{2}}. \tag{24}$$

Our analysis thoroughly examined various noise levels, as shown in Figure 2. Regularization is applied at noise levels of $p = 1\%$, $p = 3\%$, and $p = 5\%$ to understand how increasing noise affects solution stability. Figures 3 and 4 display the optimal regularization parameter λ values needed for reliable results. For **IP1**, the best λ are 10^{-2} at $p = 1\%$, 3×10^{-2} at $p = 3\%$, and 5×10^{-2} at $p = 5\%$, as seen in Figure 3. For **IP2**, they are 4×10^{-2} for $p = 1\%$, 9×10^{-2} for $p = 3\%$, and 10^{-1} for $p = 5\%$, shown in Figure 4. These findings are key to improving solution stability amid noise. Note that we did not use the L-curve method to select the regularization parameter for **IP1**. Usually, the L-curve has an L-shape, with its optimal point at the corner. Larger λ values tend to cause oversmoothing, while smaller values can result in undersmoothing; the corner indicates a balance between these two. However, in some cases, the L-curve lacks a clear corner, as noted by Hanke (1996) [25], Hansen (2001) [26], and Vogel (1996) [27]. In our case, the absence of a distinctive corner was due to the tested parameter values being very close to each other, making it difficult to identify the corner point. Conversely, the L-curve method proved effective for **IP2**. As shown in Figure 5, the optimal regularization parameter identified from the L-curve matches the value that minimizes the reconstruction error. These values are 4×10^{-2} for $p = 1\%$, 9×10^{-2} for $p = 3\%$, and 10^{-1} for $p = 5\%$.

Figures 3 to 5 present discrete numerical data computed over a limited range of regularization parameters, denoted as λ. These points are connected with straight lines to form piecewise linear curves, which may feature corners that can appear non-differentiable. However, this does not indicate non-smoothness in the true analytical solution; rather, it results from the sampling of λ and the computational approach. The V-shaped patterns in Figures 3 and 4 illustrate the trade-off between under- and over-regularization, while the corner in Figure 5 reflects the typical L-curve behavior used to choose optimal parameters. Such polygonal shapes are common in numerical implementations of Tikhonov regularization. Figures 6(a) and 6(b) compare the numerical solutions $u_0(x)$ (equation (21)) and

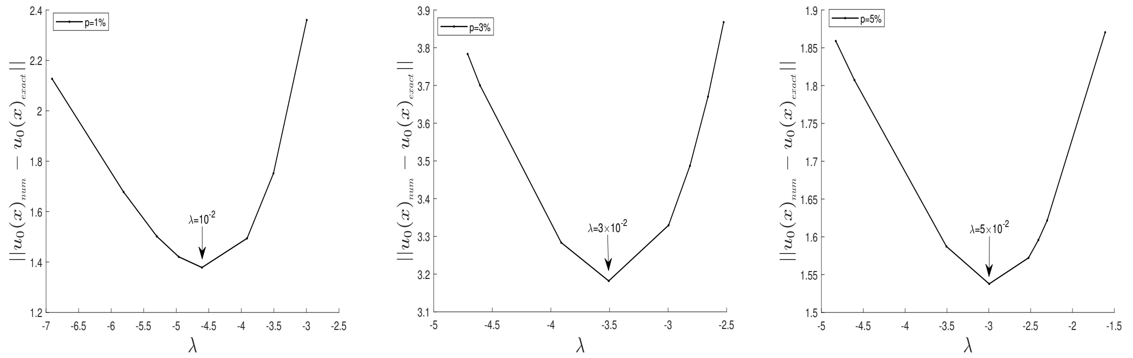

Figure 3: **IP1:** The norm error $\|u_0(x)_{\mathsf{num}} - u_0(x)_{\mathsf{exact}}\|$ (equation (23)) as a function of λ, for $M = 25$ and $N = 625$, obtained using noise levels $p = 1\%$, $p = 3\%$, and $p = 5\%$ for the inverse problem **IP1**.

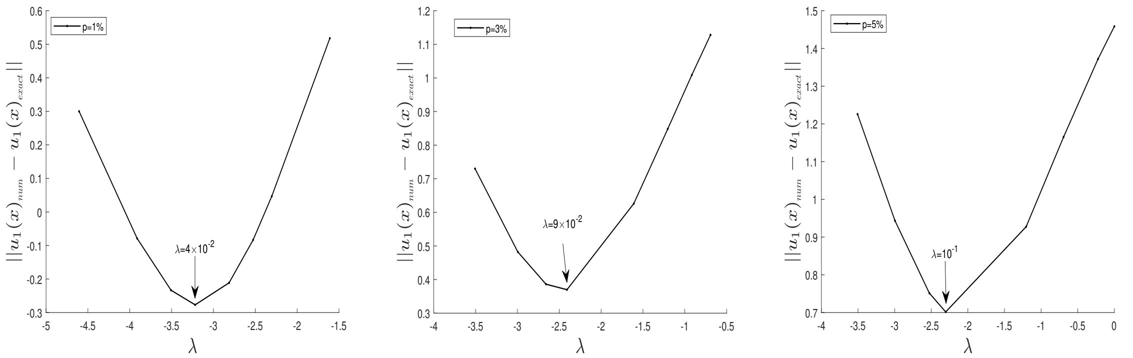

Figure 4: **IP2:** The norm error $\|u_1(x)_{\mathsf{exact}} - u_1(x)_{\mathsf{num}}\|$ (equation (24)) as a function of λ, for $M = 25$ and $N = 625$, obtained using noise levels $p = 1\%$, $p = 3\%$, and $p = 5\%$ for the inverse problem **IP2**.

$u_1(x)$ (equation (22)) with their exact counterparts $u_0(x)$ (equation (17)) and $u_1(x)$ (equation (18)). This comparison uses the optimal λ values for noise levels $p = 1\%, 3\%$, and 5%. The results confirm that the regularization method produces accurate solutions in all cases. Table 3 shows the RRMSE values for the reconstructed functions $u_0(x)$ (**IP1**) and $u_1(x)$ (**IP2**). These were calculated using the optimal regularization parameter λ at noise levels of 1%, 3%, and 5%. In both cases, the optimal regularization parameter increases with rising noise levels, indicating a need for stronger regularization for noisier data. The RRMSE values also rise as noise levels grow, reflecting the expected decline in reconstruction accuracy. Overall, both inverse problems remain stable; **IP1** shows smaller errors at low noise levels and performs similarly to **IP2** at higher noise levels.

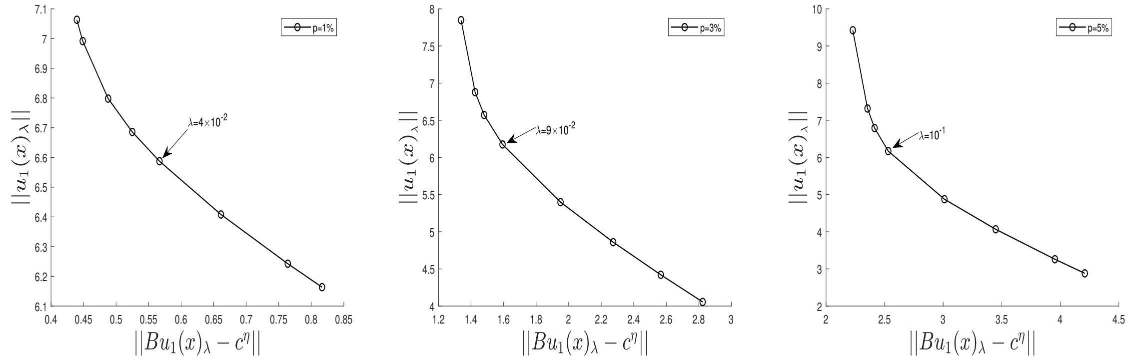

Figure 5: **IP2:** The L-curve for the Tikhonov regularization for $M = 25$ and $N = 625$, with noise levels $p \in \{1, 3, 5\}\%$, for the inverse problem **IP2**.

Table 3: RRMSE values for the reconstructed (a) $u_0(x)$ (**IP1**) and (b) $u_1(x)$ (**IP2**) obtained with the best regularization parameter λ at different noise levels.

(a) $u_0(x)$

Noise level	Best λ	RRMSE
$p = 1\%$	$\lambda = 10^{-2}$	0.097454
$p = 3\%$	$\lambda = 3 \times 10^{-2}$	0.224992
$p = 5\%$	$\lambda = 5 \times 10^{-2}$	0.329105

(b) $u_1(x)$

Noise level	Best λ	RRMSE
$p = 1\%$	$\lambda = 4 \times 10^{-2}$	0.148239
$p = 3\%$	$\lambda = 9 \times 10^{-2}$	0.204702
$p = 5\%$	$\lambda = 10^{-1}$	0.285264

5. Conclusion

This study examined inverse initial condition problems for a fourth-order partial differential equation. We used finite difference methods to discretize the governing equation in both space and time. A mesh study confirmed second-order convergence in the beam problem, showing that halving the mesh size decreased the maximum error at $T = 1$ by about four times for mesh sizes of $M = 64, 128, 256$, and 512. This approach allowed us to formulate and solve both direct and inverse problems numerically. Specifically, we examined two inverse problems: one involving inverse initial displacement and another involving inverse initial velocity. The analysis of existence and uniqueness for both direct and inverse problems was grounded in existing literature. This study also provided numerical examples to illustrate these aspects and to show the stability of the proposed method. To evaluate stability, noise (by using Gaussian normal distribution) was added to the final displacement data. As shown in the numerical examples, noise causes instability in the reconstructed solutions, as well as unstable due to the ill-conditioning of matrices $A^T A$ and $B^T B$, highlighting the ill-posed nature of inverse problems. The RRMSE was evaluated in three scenarios: prior to noise addition, after noise was added, and with the optimal Tikhonov regularization. Without noise (0%), errors were at their lowest. Adding 1% noise led to a noticeable rise in RRMSE, with further increases at 3% and 5%. The reconstruction of $u_1(x)$ was more affected by noise than $u_0(x)$, highlighting the ill-posed nature of the inverse problem. Selecting the optimal regularization enhances stability, and this optimal value generally increases with higher noise levels. Despite error

(a) (b)

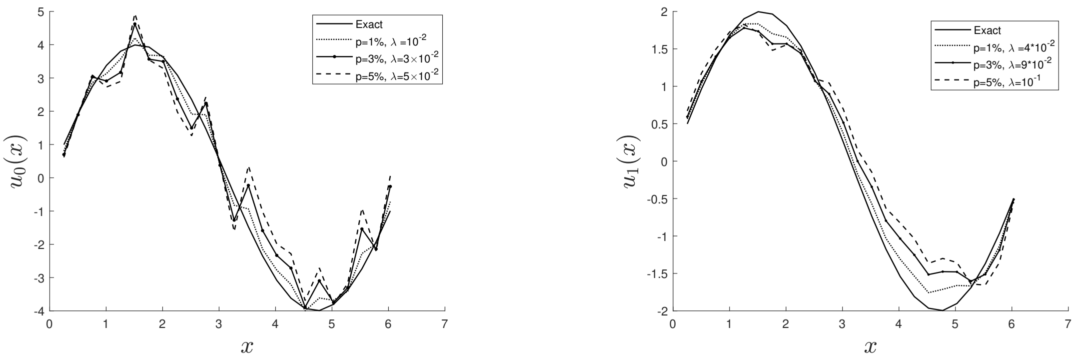

Figure 6: Comparison between (a) **IP1:** exact solution $u_0(x)$ (equation (17)) and numerical solution (equation (21)), and (b) **IP2:** exact solution $u_1(x)$ (equation (18)) and numerical solution (equation (22)), using the best λ-regularized functions, for $M = 25$, $N = 625$, and noise levels $p = \{1, 3, 5\}\%$.

growth, both inverse problems remain stable when zero-order Tikhonov regularization was applied.The optimal regularization parameter was selected by minimizing the norm error, which Figures 3 and 4 showed as a V-shape indicating the balance between under- and over-regularization. The L-curve method also aided in identifying the best regularization parameter, with the corner in Figure 5 indicating the typical L-curve behavior for choosing the optimal value, where for **IP1**, the best values were 10^{-2}, 3×10^{-2}, and 5×10^{-2} for noise levels of $1\%, 3\%$, and 5%, respectively, and for **IP2**, the corresponding values were 4×10^{-2}, 9×10^{-2}, and 10^{-1}. Future research will explore inverse initial condition problems related to second- and third-order partial differential equations.

References

[1] S. Timoshenko. *Theory of Plates and Shells.* McGraw–Hill, 1959.

[2] J. N. Reddy. *Theory and Analysis of Elastic Plates and Shells.* CRC Press, 2006.

[3] A. I. Prilepko, D. G. Orlovsky, and I. A. Vasin. *Methods for Solving Inverse Problems in Mathematical Physics.* Marcel Dekker, New York, 2000.

[4] K. B. Sabitov. A remark on the theory of initial-boundary value problems for the equation of rods and beams. *Differential Equations*, 53:86–98, 2017.

[5] K. B. Sabitov. Inverse problems of determining the right-hand side and the initial conditions for the beam vibration equation. *Differential Equations*, 56:761–774, 2020.

[6] W. B. Muniz, H. F. de Campos Velho, and F. M. Ramos. A comparison of some inverse methods for estimating the initial condition of the heat equation. *Journal of Computational and Applied Mathematics*, 103:145–163, 1999.

[7] T. Min, B. Geng, and J. Ren. Inverse estimation of the initial condition for the heat equation. *International Journal of Pure and Applied Mathematics*, 82(4):581–593, 2013.

[8] F. Yang, Y. Zhang, X.-X. Li, and C.-Y. Huang. The quasi-boundary value regular-

ization method for identifying the initial value with discrete random noise. *Boundary Value Problems*, 2018:108, 2018.

[9] U. Langer, O. Steinbach, F. Tröltzsch, and H. Yang. Space-time finite element methods for the initial temperature reconstruction. *arXiv preprint arXiv:2103.16699*, 2021.

[10] U. D. Durdiev. Inverse problem of determining an unknown coefficient in the beam vibration equation. *Differential Equations*, 58:36–43, 2022.

[11] U. D. Durdiev. Inverse problem of determining the kernel in the integro-differential beam vibration equation. *Eurasian Journal of Mathematical and Computer Applications*, 2025.

[12] S. O. Hussein. Placement inverse source problem under partition hyperbolic equation. *Iraqi Journal of Science*, 62(6):1994–1999, 2021.

[13] S. O. Hussein and M. S. Hussein. Splitting the one-dimensional wave equation, part ii: Additional data are given by an end displacement measurement. *Iraqi Journal of Science*, 62(1):233–239, 2021.

[14] S. O. Hussein. *Inverse Force Problems for the Wave Equation*. PhD thesis, University of Leeds, Leeds, UK, 2016.

[15] S. O. Hussein. Solutions for non-homogeneous wave equations subject to unusual and neumann boundary conditions. *Applied Mathematics and Computation*, 430:127285, 2022.

[16] S. O. Hussein. Inverse one-dimensional wave equation problem under upper-base as additional information. *Italian Journal of Pure and Applied Mathematics*, 47:596–608, 2022.

[17] S. A. Rashid and S. O. Hussein. The technique of analyzing a non-homogeneous partial differential equation by splitting the problem into the inverse and direct problems. *Journal of University of Babylon for Pure and Applied Sciences*, 33(4):339–362, 2021.

[18] M. J. M. Huntul. *Determination of Unknown Coefficients in the Heat Equation*. PhD thesis, University of Leeds, Leeds, UK, 2018.

[19] M. S. Hussein. *Coefficient Identification Problems in Heat Transfer*. PhD thesis, University of Leeds, Leeds, UK, 2016.

[20] I. Tekin and H. Yang. Inverse problem for the time-fractional euler–bernoulli beam equation. *Mathematical Modelling and Analysis*, 26(3):503–518, 2021.

[21] O. P. Nave. Modification of semi-analytical method applied system of ode. *Modern Applied Science*, 14(6):75, 2020.

[22] G. E. Forsythe and W. R. Wasow. *Finite-Difference Methods for Partial Differential Equations*. John Wiley, New York, 1960.

[23] R. D. Richtmyer and K. W. Morton. *Difference Methods for Initial-Value Problems*. Interscience Publishers, New York, 1967.

[24] G. D. Smith. *Numerical Solution of Partial Differential Equations: Finite Difference Methods*. Oxford University Press, 1985.

[25] M. Hanke. Limitations of the l-curve method in ill-posed problems. *BIT*, 36:287–301, 1996.

[26] P. C. Hansen. The l-curve and its use in the numerical treatment of inverse problems. In P. Johnston, editor, *Computational Inverse Problems in Electrocardiology*, pages

119–142. WIT Press, Southampton, 2001.

[27] C. R. Vogel. Non-convergence of the l-curve regularization parameter selection method. *Inverse Problems*, 12:535–547, 1996.